3D Free Vibration Analysis of Functionally Graded Plates with Arbitrary Boundary Conditions in Thermal Environment

Rui Kang, Fengxian Xin, Cheng Shen,* and Tian Jian Lu*

An analytical method for free vibration of functionally graded (FG) plates with arbitrary boundary conditions in thermal environments is developed based on 3D elasticity theory. Material properties of the FG plate are assumed to be temperature dependent but graded along with its thickness. At the edges of the plate, three different sets of linear springs are introduced, so that its boundary condition can be altered by changing the spring stiffness. Each displacement component of the plate is expanded as a standard Fourier cosine series, supplemented with closed-form auxiliary functions. With thermal environment effects duly accounted for, the energy method is used to derive eigenvalue equations, whereas the Rayleigh–Ritz procedure is utilized to calculate the natural frequencies of the FG plate. Numerical examples show that the present method converges quickly and gives satisfactory results. The method is then utilized to calculate the natural frequencies of FG plates having different aspect ratios, volume fractions, and elastic boundaries.

1. Introduction

Functionally graded materials (FGMs) have been proposed to overcome severe aerodynamic heating encountered by aerocraft (e.g., supersonic aircraft).[1] FGMs are typically heterogeneous, with properties varying continuously and smoothly. In addition to thermal protection, functionally graded (FG) electroactive materials and magnetoactive materials for sensors, actuators, biomedical devices, and flexible electronics have been exploited.[2,3] Further, FG graphene/carbon nanotube-reinforced materials with high strength/stiffness have been extensively studied.[4,5] Until now, the most popular FGM is composed of ceramic and metal materials; the benefit is that it can enjoy both

the low thermal conductivity of ceramic and the high toughness of metal to prevent premature ceramic cracking. With great achievements in the past decades, the FG plates constitute a basic structural form and have been widely applied in complex environments where, in addition to requiring high stiffness/strength, thermal vibration is also of significant concern.

To characterize the vibration properties of an FG plate, a variety of plate theories have been developed. For instance, the thermal free vibration of exponential FG rectangular plates, FG thin annular sector plates, and FG circular plates were analyzed using the classical plate theory.[6–8] While high accuracy was achieved in thin plates, the analysis error increases with plate thickness, because the effects of shear and normal deformations in thickness direction were neglected. For moderately thick and thick FG plates, the first-order shear deformation theory was proposed.[9–11] Nonetheless, as the transverse shear strain is assumed to be constant along with plate thickness, a shear correction factor must be introduced to correct errors caused by nonzero shear stresses on free surfaces. To avoid the use of the shear correction factor, a variety of higher-order plate theories were proposed.[12–16] In addition to plate theories, the theory of 3D elasticity is also widely to analyze the vibration of rectangular and annular FG plates.[17–19] As no assumptions about the distribution of deformation and stress are made, the 3D elasticity theory is deemed more accurate than the higher-order plate theories.

The 3D elasticity theory can be used to systematically investigate how boundary conditions affect the free vibration of an FG plate, as existing analyses only considered idealized boundary conditions, such as free, simply supported, clamped, or their combinations. In practice, most engineering structures are not absolutely free, simply supported, or clamped, but may have boundary conditions closer to elastic. For both monolithic and FG plates, the effects of elastic-constraint boundary conditions on plate vibration have already been analyzed.[20–30] However, for an FG plate constrained elastically at its edges by springs,[29,30] how its frequency parameters change under varying temperature environments remains elusive.

Built upon the 3D elasticity theory, this study aims to analyze the free vibration of an FG plate having arbitrary boundary conditions in thermal environments, with temperature effects accounted for from two aspects: temperature-dependent material

R. Kang, C. Shen, T. J. Lu
State Key Laboratory of Mechanics and Control of Mechanical Structures
MIIT Key Laboratory of Multifunctional Lightweight Materials and Structures (MLMS)
Nanjing University of Aeronautics and Astronautics
Nanjing 210016, China
E-mail: cshen@nuaa.edu.cn; tjlu@nuaa.edu.cn

F. Xin
State Key Laboratory for Strength and Vibration of Mechanical Structures
Xi'an Jiaotong University
Xi'an 710049, China

The ORCID identification number(s) for the author(s) of this article can be found under https://doi.org/10.1002/adem.202100636.

**ADVANCED
SCIENCE NEWS**
www.advancedsciencenews.com

**ADVANCED
ENGINEERING
MATERIALS**
www.aem-journal.com

properties and thermal strain energy caused by elastic constraints. With three different sets of springs introduced to characterize elastic constraints at plate edges and the displacement components expanded into improved Fourier series, the free vibration problem is solved using the Rayleigh–Ritz method. For validation, natural frequencies calculated under classical boundary conditions are compared with existing results. The proposed method is then utilized to quantify the influences of plate aspect ratio, volume fraction, and elastic constraints and explore the vibration characteristics of FG plates in thermal environments.

2. Theoretical Formulation

2.1. Geometrical Configuration

Figure 1 shows the FG plate of concern, together with the coordinate system for analysis. Let its length, width, and thickness be denoted by a, b, and h, and let u, v, and w represent its displacement components in the x, y, and z directions, respectively. With the equivalent stiffness of the elastically restrained plate edges represented by three sets of independent springs (denoted herein by ku, kv, and kw), boundary conditions of the plate can be systematically adjusted by varying individual spring stiffness. For example, the classical clamped and free boundaries can be modeled by setting the related spring stiffness to approach infinity and zero, respectively. Values of spring stiffness suitable for representative boundary conditions are provided in subsequent sections (e.g., Table A.2 in Appendix A).

2.2. Material Properties

According to the definition of an FG plate, the properties of its material can vary continuously along the thickness direction as the volume fractions of its constituents are varied. In the current study, the FG plate is composed of ceramic and metal materials, as shown in Figure 1. For simplicity, the FG is assumed to have a uniform temperature T, the same as the environment. Existing researches on free vibration of FG plates revealed that the influence of uniform temperature on natural frequencies is more significant than nonuniform temperature.[6,12,17]

Material properties of the FG plate are assumed to vary in its thickness direction as

$$P(z, T) = P_{\mathrm{m}}(T) + (P_{\mathrm{c}}(T) - P_{\mathrm{m}}(T))\left(\frac{z}{h}\right)^p \tag{1}$$

where T is the temperature and $P(z, T)$ represents material parameters of the FG plate, such as Young's modulus $E(z, T)$, Poisson ratio $v(z, T)$, mass density $\rho(z, T)$, and thermal expansion coefficient $\alpha(z, T)$. $P_{\mathrm{m}}(T)$ and $P_{\mathrm{c}}(T)$ are temperature-dependent material properties of ceramic and metal, respectively. Different values of the volume fraction index p represent different material distributions along with plate thickness: the pure ceramic plate is obtained by setting p to zero, whereas the pure metal plate is recovered by setting p to infinite.

Temperature-dependent material properties are taken as nonlinear functions of temperature, given by[31]

$$P(T) = P_0(P_{-1}T^{-1} + 1 + P_1 T + P_2 T^2 + P_3 T^3) \tag{2}$$

where P_0, P_{-1}, P_1, P_2, and P_3 are temperature coefficients, with specific values shown in Table A.1 for selected materials,[32] and $T = T_0 + \Delta T(z)$, $T_0 = 300\ \mathrm{K}$ being room temperature.

2.3. Constitutive Laws and Kinematic Relations

For the FG plate of concern, the 3D elastic constitutive relations can be written as

$$\begin{Bmatrix} \sigma_{xx} \\ \sigma_{yy} \\ \sigma_{zz} \\ \sigma_{xy} \\ \sigma_{xz} \\ \sigma_{yz} \end{Bmatrix} = \begin{bmatrix} A & B & B & 0 & 0 & 0 \\ B & A & B & 0 & 0 & 0 \\ B & B & A & 0 & 0 & 0 \\ 0 & 0 & 0 & C & 0 & 0 \\ 0 & 0 & 0 & 0 & C & 0 \\ 0 & 0 & 0 & 0 & 0 & C \end{bmatrix} \begin{Bmatrix} \varepsilon_{xx} \\ \varepsilon_{yy} \\ \varepsilon_{zz} \\ \gamma_{xy} \\ \gamma_{xz} \\ \gamma_{yz} \end{Bmatrix} \tag{3}$$

where the reduced stiffness coefficients are

$$A = \frac{E(z,T)v(z,T)}{(1 + v(z,T))(1 - 2v(z,T))} + \frac{E(z,T)}{1 + v(z,T)}$$
$$B = \frac{E(z,T)v(z,T)}{(1 + v(z,T))(1 - 2v(z,T))} \quad C = \frac{E(z,T)}{2(1 + v(z,T))} \tag{4}$$

In accordance with linear, small-strain elasticity theory, strain components are defined as

$$\varepsilon_{xx} = \frac{\partial u}{\partial x}; \quad \varepsilon_{yy} = \frac{\partial v}{\partial y}; \quad \varepsilon_{zz} = \frac{\partial w}{\partial z}; \quad \gamma_{xy} = \frac{\partial u}{\partial y} + \frac{\partial v}{\partial x};$$
$$\gamma_{xz} = \frac{\partial u}{\partial z} + \frac{\partial w}{\partial x}; \quad \gamma_{yz} = \frac{\partial v}{\partial z} + \frac{\partial w}{\partial y} \tag{5}$$
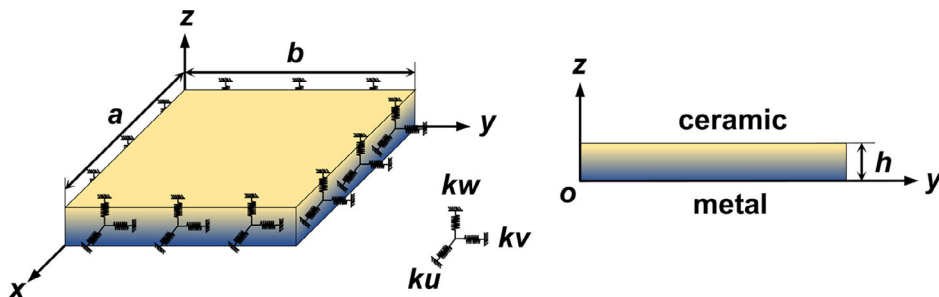
Figure 1. Schematic of an FG plate with elastically restrained edges represented by three independent sets of springs.

2.4. Energy Expressions

The strain energy U_e of the FG plate is given by

$$U_e = \frac{1}{2}\int_V (\sigma_{xx}\varepsilon_{xx} + \sigma_{yy}\varepsilon_{yy} + \sigma_{zz}\varepsilon_{zz} + \sigma_{xy}\gamma_{xy} + \sigma_{yz}\gamma_{yz} + \sigma_{xz}\gamma_{xz})\mathrm{d}V \tag{6}$$

where V is the volume of the plate. Detailed expression of U_e can be obtained by substituting (3)–(5) into (6), yielding

$$\begin{aligned}
U_e = \frac{1}{2}\int_0^a\int_0^b\int_0^h &\left\{ A\left[\left(\frac{\partial u}{\partial x}\right)^2 + \left(\frac{\partial v}{\partial y}\right)^2 + \left(\frac{\partial w}{\partial z}\right)^2\right] \right.\\
&+ 2B\left(\frac{\partial u}{\partial x}\frac{\partial v}{\partial y} + \frac{\partial u}{\partial x}\frac{\partial w}{\partial z} + \frac{\partial v}{\partial y}\frac{\partial w}{\partial z}\right)\\
&+ C\left[\left(\frac{\partial u}{\partial y}\right)^2 + \left(\frac{\partial v}{\partial x}\right)^2 + \left(\frac{\partial u}{\partial z}\right)^2 + \left(\frac{\partial w}{\partial x}\right)^2 \right.\\
&\left. + \left(\frac{\partial v}{\partial z}\right)^2 + \left(\frac{\partial w}{\partial y}\right)^2\right]\\
&\left. + 2C\left(\frac{\partial u}{\partial y}\frac{\partial v}{\partial x} + \frac{\partial u}{\partial z}\frac{\partial w}{\partial x} + \frac{\partial v}{\partial z}\frac{\partial w}{\partial y}\right)\right\}\mathrm{d}x\mathrm{d}y\mathrm{d}z
\end{aligned} \tag{7}$$

The elastic potential energy stored in the springs can be expressed as

$$\begin{aligned}
U_{\mathrm{spring}} = \frac{1}{2}\int_0^h\int_0^b &[(ku_{x0} + ku_{xa})u^2 + (kv_{x0} + kv_{xa})v^2\\
&+ (kw_{x0} + kw_{xa})w^2]\mathrm{d}y\mathrm{d}z\\
+ \frac{1}{2}\int_0^h\int_0^a &[(ku_{y0} + ku_{yb})u^2 + (kv_{y0} + kv_{yb})v^2\\
&+ (kw_{y0} + kw_{yb})w^2]\mathrm{d}x\mathrm{d}z
\end{aligned} \tag{8}$$

where $x0$, xa, $y0$, and yb indicate the positions of springs. For example, $x0$ and xa indicate that the springs are distributed along the edge $x = 0$ and edge $x = a$, respectively.

Kinetic energy T_e of the FG plate is

$$T_e = \frac{1}{2}\int_V \rho(z,T)\left(\left(\frac{\partial u}{\partial t}\right)^2 + \left(\frac{\partial v}{\partial t}\right)^2 + \left(\frac{\partial w}{\partial t}\right)^2\right)\mathrm{d}V \tag{9}$$

Thermal stresses in the FG plate can be expressed as

$$\begin{Bmatrix}\sigma_{0xx}\\\sigma_{0yy}\\\sigma_{0zz}\\\sigma_{0xy}\\\sigma_{0xz}\\\sigma_{0yz}\end{Bmatrix} = \begin{bmatrix}A & B & B & 0 & 0 & 0\\B & A & B & 0 & 0 & 0\\B & B & A & 0 & 0 & 0\\0 & 0 & 0 & C & 0 & 0\\0 & 0 & 0 & 0 & C & 0\\0 & 0 & 0 & 0 & 0 & C\end{bmatrix}\begin{Bmatrix}-\alpha(z,T)\Delta T\\-\alpha(z,T)\Delta T\\-\alpha(z,T)\Delta T\\0\\0\\0\end{Bmatrix} \tag{10}$$

whereas thermal strains caused by temperature variation can be written as[6]

$$\begin{aligned}
d_{xx} &= \frac{\partial u}{\partial x}\frac{\partial u}{\partial x} + \frac{\partial v}{\partial x}\frac{\partial v}{\partial x} + \frac{\partial w}{\partial x}\frac{\partial w}{\partial x}\\
d_{yy} &= \frac{\partial u}{\partial y}\frac{\partial u}{\partial y} + \frac{\partial v}{\partial y}\frac{\partial v}{\partial y} + \frac{\partial w}{\partial y}\frac{\partial w}{\partial y}\\
d_{xy} &= \frac{\partial u}{\partial x}\frac{\partial u}{\partial y} + \frac{\partial v}{\partial x}\frac{\partial v}{\partial y} + \frac{\partial w}{\partial x}\frac{\partial w}{\partial y}
\end{aligned} \tag{11}$$

The strain energy of initial thermal stresses induced by temperature rise ΔT is thus

$$U_T = \frac{1}{2}\int_V (\sigma_{0xx}d_{xx} + \sigma_{0yy}d_{yy} + 2\sigma_{0xy}d_{xy})\mathrm{d}V \tag{12}$$

Deformation of FG plate along z-direction is not constrained; thus, thermal strain energy containing the z-coordinate is ignored in (12). Detailed expression of U_T can thence be obtained by substituting (10) and (11) into (12), yielding

$$\begin{aligned}
U_T = \int_0^a\int_0^b\int_0^h &-\frac{1}{2}(A + 2B)\left(\frac{\partial u}{\partial x}\frac{\partial u}{\partial x} + \frac{\partial v}{\partial x}\frac{\partial v}{\partial x}\right.\\
&+ \frac{\partial w}{\partial x}\frac{\partial w}{\partial x} + \frac{\partial u}{\partial y}\frac{\partial u}{\partial y} + \frac{\partial v}{\partial y}\frac{\partial v}{\partial y} + \frac{\partial w}{\partial y}\frac{\partial w}{\partial y}\right)\\
&\times \alpha(z,T)\Delta T\mathrm{d}x\mathrm{d}y\mathrm{d}z
\end{aligned} \tag{13}$$

2.5. Admissible Displacement Functions and Solution Procedure

Modified 3D Fourier cosine series supplemented with closed-form auxiliary functions are selected as the displacement functions that satisfy arbitrary boundary conditions,[28] namely

$$\begin{aligned}
u(x,y,z,t) = &\left(\sum_{m=0}^\infty\sum_{n=0}^\infty\sum_{l=0}^\infty A_{mnl}H_{xyz} + \sum_{m=0}^\infty\sum_{n=0}^\infty\sum_{r=1}^2 a_{mnr}H_{xy\xi_{rz}}\right.\\
&\left. + \sum_{m=0}^\infty\sum_{r=1}^2\sum_{l=0}^\infty a_{mrl}H_{x\xi_{ry}z} + \sum_{r=1}^2\sum_{n=0}^\infty\sum_{l=0}^\infty a_{rnl}H_{\xi_{rx}yz}\right)e^{i\omega t}
\end{aligned} \tag{14}$$

$$\begin{aligned}
v(x,y,z,t) = &\left(\sum_{m=0}^\infty\sum_{n=0}^\infty\sum_{l=0}^\infty B_{mnl}H_{xyz} + \sum_{m=0}^\infty\sum_{n=0}^\infty\sum_{r=1}^2 b_{mnr}H_{xy\xi_{rz}}\right.\\
&\left. + \sum_{m=0}^\infty\sum_{r=1}^2\sum_{l=0}^\infty b_{mrl}H_{x\xi_{ry}z} + \sum_{r=1}^2\sum_{n=0}^\infty\sum_{l=0}^\infty b_{rnl}H_{\xi_{rx}yz}\right)e^{i\omega t}
\end{aligned} \tag{15}$$

$$\begin{aligned}
w(x,y,z,t) = &\left(\sum_{m=0}^\infty\sum_{n=0}^\infty\sum_{l=0}^\infty C_{mnl}H_{xyz} + \sum_{m=0}^\infty\sum_{n=0}^\infty\sum_{r=1}^2 c_{mnr}H_{xy\xi_{rz}}\right.\\
&\left. + \sum_{m=0}^\infty\sum_{r=1}^2\sum_{l=0}^\infty c_{mrl}H_{x\xi_{ry}z} + \sum_{r=1}^2\sum_{n=0}^\infty\sum_{l=0}^\infty c_{rnl}H_{\xi_{rx}yz}\right)e^{i\omega t}
\end{aligned} \tag{16}$$

where A_{mnl}, B_{mnl}, C_{mnl}, a_{mnr}, b_{mnr}, c_{mnr}, a_{mrl}, b_{mrl}, c_{mrl}, a_{rnl}, b_{rnl}, and c_{rnl} are unknown coefficients, and ω is the natural frequency of FG plate, with i representing the imaginary unit and t the time variable. The expanded series functions can be expressed as

$$H_{xyz} = \cos\lambda_m x \cos\lambda_n y \cos\lambda_l z \quad H_{xy\xi_{rz}} = \cos\lambda_m x \cos\lambda_n y \xi_{rz}(z)$$

$$H_{x\xi_{ry}z} = \cos\lambda_m x \xi_{ry}(y)\cos\lambda_l z \quad H_{\xi_{rx}yz} = \xi_{rx}(x)\cos\lambda_n y \cos\lambda_l z$$

$$\lambda_m = m\pi/a \quad \lambda_n = n\pi/b \quad \lambda_l = l\pi/h$$

$$(17)$$

where the closed-form auxiliary functions are

$$\xi_{rx}(x) = \begin{cases} x\left(\dfrac{x}{a}-1\right)^2 & r=1 \\[2mm] \dfrac{x^2}{a}\left(\dfrac{x}{a}-1\right) & r=2 \end{cases} \tag{18}$$

$$\xi_{ry}(y) = \begin{cases} y\left(\dfrac{y}{b}-1\right)^2 & r=1 \\[2mm] \dfrac{y^2}{b}\left(\dfrac{y}{b}-1\right) & r=2 \end{cases} \tag{19}$$

$$\xi_{rz}(z) = \begin{cases} z\left(\dfrac{z}{h}-1\right)^2 & r=1 \\[2mm] \dfrac{z^2}{h}\left(\dfrac{z}{h}-1\right) & r=2 \end{cases} \tag{20}$$

It is worth noting that the form of auxiliary function is not unique. Any type of closed function satisfying the following conditions can be used to deal with possible discontinuities of displacement or derivatives at the edges of the plate

$$\xi_{1x}(0) = \xi_{1x}(a) = \xi'_{1x}(a) = 0, \quad \xi'_{1x}(0) = 1 \tag{21}$$

$$\xi_{2x}(0) = \xi_{2x}(a) = \xi'_{2x}(a) = 0, \quad \xi'_{2x}(a) = 1 \tag{22}$$

$$\xi_{1y}(0) = \xi_{1y}(b) = \xi'_{1y}(b) = 0, \quad \xi'_{1y}(0) = 1 \tag{23}$$

$$\xi_{2y}(0) = \xi_{2y}(b) = \xi'_{2y}(0) = 0, \quad \xi'_{2y}(b) = 1 \tag{24}$$

$$\xi_{1z}(0) = \xi_{1z}(h) = \xi'_{1z}(h) = 0, \quad \xi'_{1z}(0) = 1 \tag{25}$$

$$\xi_{2z}(0) = \xi_{2z}(h) = \xi'_{2z}(0) = 0, \quad \xi'_{2z}(h) = 1 \tag{26}$$

The first-order displacement derivative has auxiliary terms only at the edge. In other words, the potential discontinuity of the first-order displacement derivative at the edge is effectively transferred to the auxiliary functions.

Finally, detailed displacement functions can be obtained by substituting (17)–(20) into (14)–(16). Once the displacement field is expressed using a suitable form like (14)–(16), the remaining task is to determine the unknown coefficients. A conventional solution strategy is substituting the assumed displacement field into the governing equation and boundary conditions, which is effective but cumbersome. The Rayleigh–Ritz solution procedure is used instead in the present work, with a flowchart shown in **Figure 2**.

The Lagrangian function of the FG plate system can be expressed as

$$\Pi = T_e - U_e - U_{\text{spring}} - U_T \tag{27}$$

where the kinetic energy T_e, the strain energy of plate U_e, the potential energy of spring U_{spring}, and the thermal strain energy U_T have been defined in (7)–(9) and (13), respectively. Substituting these four equations into (27) and minimizing the Lagrangian function against all unknown coefficients lead to

$$\frac{\partial\Pi}{\partial\eta} = 0 \quad \eta = A_{mnl}, a_{mnr}, a_{mrl}, a_{rnl}, B_{mnl}, b_{mnr}, b_{mrl}, b_{rnl},$$
$$C_{mnl}, c_{mnr}, c_{mrl}, c_{rnl} \tag{28}$$

Calculate the strain energy (U_e), elastic potential energy (U_{spring}) of artificial spring, kinetic energy (T_e) and thermal strain energy (U_T) caused by temperature change

Expand the displacement fields u, v and w into improved three dimensional Fourier series:
$$u(x,y,z,t) = (\sum_{m=0}^{\infty}\sum_{n=0}^{\infty}\sum_{l=0}^{\infty}A_{mnl}H_{xyz} + \sum_{m=0}^{\infty}\sum_{n=0}^{\infty}\sum_{r=1}^{2}a_{mnr}H_{xy\xi_{rz}} + \sum_{m=0}^{\infty}\sum_{r=1}^{2}\sum_{l=0}^{\infty}a_{mrl}H_{x\xi_{ry}z} + \sum_{r=1}^{2}\sum_{n=0}^{\infty}\sum_{l=0}^{\infty}a_{rnl}H_{\xi_{rx}yz})e^{i\omega t}$$

Substitute the expanded displacement fields into the Lagrangian energy expression:
$$\Pi = T_e - U_e - U_{spring} - U_T$$

Minimize the Lagrangian energy expression against all unknown coefficients:
$$\frac{\partial\Pi}{\partial\eta} = 0 \quad \eta = A_{mnl}, a_{mnr}, a_{mrl}, a_{rnl}, B_{mnl}, b_{mnr}, b_{mrl}, b_{rnl}, C_{mnl}, c_{mnr}, c_{mrl}, c_{rnl}$$
The free vibration problem can be transformed into a standard matrix eigenvalue problem

Solve the eigenvalue problem:
$$([K]+[K_S]+[K_T]-\omega^2[M])\{\Phi\} = \{0\}$$
The solution of the eigenvalue problem gives the natural frequency parameters ω and mode shapes Φ

Figure 2. Flowchart of the Rayleigh–Ritz solution procedure.

Finally, upon transforming the free vibration problem into a standard matrix eigenvalue problem, the following governing equations are obtained

$$([K] + [K_S] + [K_T] - \omega^2[M])\{\Phi\} = \{0\} \tag{29}$$

where $[K]$ is the symmetric stiffness matrix obtained from the strain energy of the plate, $[K_S]$ is the stiffness matrix obtained from the potential energy of the springs, $[K_T]$ is the stiffness matrix obtained from the strain energy of initial thermal stresses induced by temperature rise, and $[M]$ is the mass matrix. Φ is the column vector of unknown coefficients

$$\{\Phi\}^T = \{A_{mnl}, a_{mnr}, a_{mrl}, a_{rnl}, B_{mnl}, b_{mnr}, b_{mrl}, b_{rnl}, C_{mnl}, \\ c_{mnr}, c_{mrl}, c_{rnl}\} \tag{30}$$

Detailed expressions of these matrices can be found in Appendix B. Ultimately, the solution of the eigenvalue problem, Equation (29), gives the natural frequency parameters and mode shapes of the FG plate in thermal environments.

3. Numerical Results and Discussion

3.1. Determination of Spring Stiffness

As shown in Figure 1, three sets of springs are assigned to the edges of the FG plate to restrain its displacement in three coordinate directions. Theoretically, when all springs are set to have infinite (or zero) stiffness, the boundary condition becomes clamped (or free). As numerical calculations cannot deal with infinite values directly, spring stiffness must be reasonably set to ensure sufficient calculation accuracy. For illustration, for a clamped FG plate, **Table 1** shows how spring stiffness (ku, kv, and kw) affects the convergence of nondimensional natural frequency λ, defined as

$$\lambda = \omega b^2/\pi^2 \sqrt{(\rho_0 h)/D_0} \quad D_0 = E_0 h^3/[12(1 - \nu_0^2)] \tag{31}$$

where ρ_0, E_0, and ν_0 refer to the mass density, Young's modulus, and Poisson ratio of SUS304 at 300 K (Table A.1), respectively. Unless specifically noted, all the natural frequencies in subsequent numerical examples are denoted in the nondimensional form of (31).

The results of Table 1 show that, when the spring stiffness is greater than 1e-19, the first eight natural frequencies converge gradually. Values of spring stiffness associated with the three classical boundary conditions, that is, free (referred to as F), simply supported (referred to as S), and clamped (referred to as C), are shown in Table A.2. It is worth emphasizing that the present model can be used to deal with situations where the four plate edges have different restraint conditions, for example, one boundary simply supported and the others clamped (SCCC). This is the main reason why "arbitrary" is used in the title of this study.

Table 1. Determination of spring stiffness for CCCC FG square plates with different thickness-side ratios ($T_0 = 300$ K, $\Delta T = T - T_0 = 0$ K).

h/b	$ku = kv = kw$ [N/m]	Natural frequency
		λ_1	λ_2	λ_3	λ_4	λ_5	λ_6	λ_7	λ_8
0.05	1e-12	2.3060	5.4042	5.4042	8.1736	10.2319	10.2531	12.0003	12.0003
	1e-13	3.0744	6.4590	6.4590	9.6066	11.7355	11.7673	14.6705	14.6705
	1e-14	3.8340	7.6775	7.6775	11.1385	13.4137	13.4936	16.5929	16.5929
	1e-16	4.0345	8.0531	8.0531	11.6503	14.0160	14.1060	17.3002	17.3002
	1e-18	4.0540	8.0923	8.0923	11.7065	14.0824	14.1734	17.3804	17.3804
	1e-19	4.0545	8.0933	8.0933	11.7079	14.0840	14.1751	17.3824	17.3824
	1e-20	4.0545	8.0934	8.0934	11.7080	14.0842	14.1752	17.3826	17.3826
0.1	1e-12	2.1102	4.6585	4.6585	6.0010	6.0010	6.6593	8.0117	8.1705
	1e-13	2.9067	5.8705	5.8705	8.4474	10.1422	10.1937	11.5152	11.5152
	1e-14	3.5757	6.8480	6.8480	9.6311	11.3616	11.4584	13.5323	13.5323
	1e-16	3.7462	7.1339	7.1339	9.9889	11.7582	11.8733	13.8438	13.8438
	1e-18	3.7558	7.1513	7.1513	10.0116	11.7842	11.9004	13.8516	13.8516
	1e-19	3.7560	7.1516	7.1516	10.0119	11.7846	11.9007	13.8518	13.8518
	1e-20	3.7560	7.1516	7.1516	10.0119	11.7846	11.9008	13.8518	13.8518
0.5	1e-12	0.9929	1.1918	1.1918	1.5740	1.5740	1.6890	2.0667	2.2162
	1e-13	1.4882	2.2592	2.2592	2.4409	2.4409	2.8801	3.1590	3.3135
	1e-14	1.6675	2.6056	2.6056	2.6828	2.6828	3.1339	3.4256	3.7589
	1e-16	1.7042	2.6504	2.6504	2.7337	2.7337	3.1632	3.4693	3.8330
	1e-18	1.7047	2.6510	2.6510	2.7343	2.7343	3.1635	3.4699	3.8339
	1e-19	1.7047	2.6510	2.6510	2.7343	2.7343	3.1635	3.4699	3.8340
	1e-20	1.7047	2.6510	2.6510	2.7343	2.7343	3.1635	3.4699	3.8340

ADVANCED
SCIENCE NEWS
www.advancedsciencenews.com

ADVANCED
ENGINEERING
MATERIALS
www.aem-journal.com

Table 2. Convergence study of nondimensional natural frequency λ for an SSSS FG plate subjected to uniform temperature rise ($T_0 = 300$ K, $\Delta T = T - T_0$).

ΔT [K]	$M \times N \times L$	Natural frequency							
		λ_1	λ_2	λ_3	λ_4	λ_5	λ_6	λ_7	λ_8
0	$4 \times 4 \times 2$	2.7276	6.1973	6.1973	8.1041	8.1041	9.7522	11.4501	13.5178
	$8 \times 8 \times 4$	2.4189	5.7594	5.7594	8.1033	8.1033	8.8611	10.7653	10.7988
	$12 \times 12 \times 6$	2.4031	5.7360	5.7360	8.1033	8.1033	8.8134	10.7351	10.7417
	$16 \times 16 \times 8$	2.4007	5.7322	5.7322	8.1033	8.1033	8.8053	10.7311	10.7332
	$17 \times 17 \times 8$	2.4004	5.7319	5.7319	8.1033	8.1033	8.8051	10.7306	10.7320
	$18 \times 18 \times 9$	2.4003	5.7316	5.7316	8.1033	8.1033	8.8040	10.7305	10.7318
300	$4 \times 4 \times 2$	2.2609	5.5936	5.5936	7.7330	7.7330	9.0234	10.9252	12.7572
	$8 \times 8 \times 4$	1.9139	5.1446	5.1446	7.7323	7.7323	8.1283	9.9567	9.9894
	$12 \times 12 \times 6$	1.8955	5.1204	5.1204	7.7323	7.7323	8.0801	9.9257	9.9322
	$16 \times 16 \times 8$	1.8927	5.1165	5.1165	7.7323	7.7323	8.0719	9.9215	9.9235
	$17 \times 17 \times 8$	1.8923	5.1162	5.1162	7.7323	7.7323	8.0718	9.9211	9.9224
	$18 \times 18 \times 9$	1.8923	5.1159	5.1159	7.7323	7.7323	8.0706	9.9209	9.9222
600	$4 \times 4 \times 2$	1.3472	4.5410	4.5410	7.0279	7.0279	7.7522	9.9253	11.5186
	$8 \times 8 \times 4$	0.7733	4.0574	4.0574	6.8394	7.0273	7.0273	8.5287	8.5598
	$12 \times 12 \times 6$	0.7337	4.0306	4.0306	6.7895	7.0273	7.0273	8.4948	8.5011
	$16 \times 16 \times 8$	0.7273	4.0263	4.0263	6.7810	7.0273	7.0273	8.4903	8.4922
	$17 \times 17 \times 8$	0.7265	4.0260	4.0260	6.7809	7.0273	7.0273	8.4897	8.4910
	$18 \times 18 \times 9$	0.7264	4.0256	4.0256	6.7796	7.0273	7.0273	8.4896	8.4908

3.2. Convergence Study

When using the method of series expansion, it is necessary to conducted a convergence study. Moreover, the effect of temperature on the convergence of improved Fourier series is yet to be analyzed, although its convergence in the absence of thermal effects has been established.[28] In this section, to check the convergence of the present numerical method, an SSSS FG plate is taken as a representative example, with its geometrical dimensions given by: length $a = b = 0.2$ m, thickness-side ratio $h/b = 0.1$, and volume fraction index $p = 2$. As shown in **Table 2**, when the truncated numbers in the improved Fourier series are greater than $16 \times 16 \times 8$, the relative error of nondimensional natural frequency λ does not exceed 0.11% for all the temperature conditions considered. For other types of boundary conditions, it is found that selecting $16 \times 16 \times 8$ also ensures convergence (details not shown for brevity). Therefore, in all subsequent calculations, the truncated numbers are selected as $M \times N \times L = 16 \times 16 \times 8$ by default.

3.3. Validation of Analytical Method: Isotropic Plates with Classical Boundary Conditions

To validate the analytical method, obtained results are compared with those calculated using alternative methods, first, for isotropic plates and then for FG plates. To this end, Table A.3 shows the first seven frequency parameters (θ) for isotropic Al_2O_3 square plates having varying thickness-side ratios ($h/b = 0.1$, 0.2, 0.5), with θ defined by

$$\theta = \omega b^2 \sqrt{12\rho(1 - v^2)/(Eh^2)} \qquad (32)$$

Relevant material and geometric parameters are $E = 380$ GPa, $v = 0.3$, $\rho = 3800$ kg m^{-3}, length $a = 0.2$ m, aspect ratios $a/b = 1.0$, and volume fraction index $p = 0$. Three classical boundary conditions, that is, FFFF, SSSS, and CCCC, are selected. It is seen from Table A.3 that the present calculation results are in excellent agreement with existing results.[28,33,34] In addition, **Figure 3–5** shows the first six 3D mode shapes of isotropic Al_2O_3 square plates (with thickness-side ratio fixed at 0.1), under FFFF, SSSS, and CCCC boundary conditions.

3.4. Validation of Analytical Method: FG Plates in Thermal Environment

For further validation, especially for thermal applications, the nondimensional natural frequencies of CCCC Si_3N_4/SUS304 FG plates are compared with existing results.[14,17,35] In Table A.4, an FG square plate ($a = b = 0.2$ m, $h/b = 0.1$, and $p = 2$) is subjected to different temperature increases: $\Delta T = 0$ K, 300 K, 500 K. In Table A.5, a square FG plate has fixed length $a = 0.2$ m and thickness-to-length ratio $h/b = 0.1$, whereas its volume fraction index p and aspect ratio a/b are both varied; the temperature rise is set as $\Delta T = 300$ K. Similar to the case of isotropic plates, the results of Table A.4 and A.5 demonstrate again that the present results for FG plates in thermal environments agree well with those reported by others.[14,17,35]
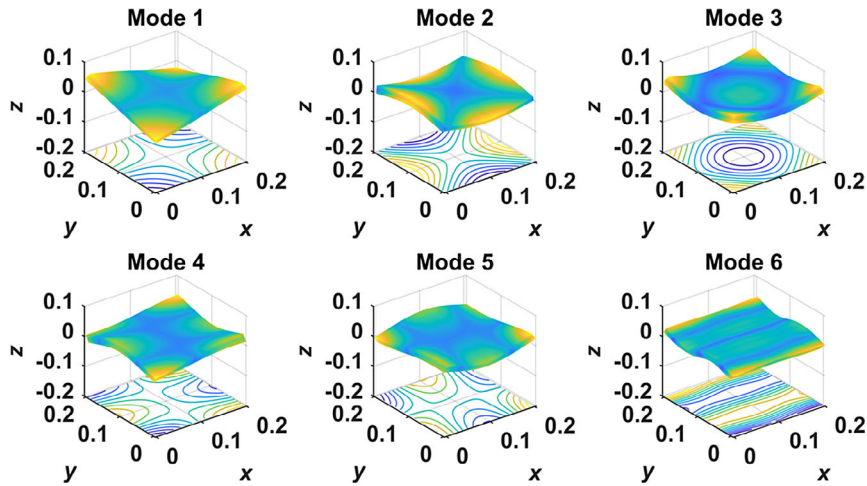
Figure 3. The first six 3D mode shapes of FFFF Al_2O_3 square plate with thickness-side ratio fixed at 0.1.
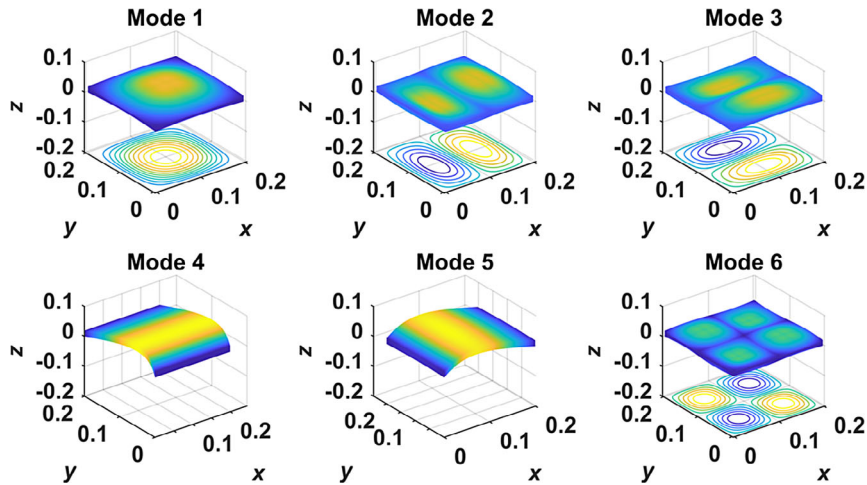
Figure 4. The first six 3D mode shapes of SSSS Al_2O_3 square plate with thickness-side ratio fixed at 0.1.
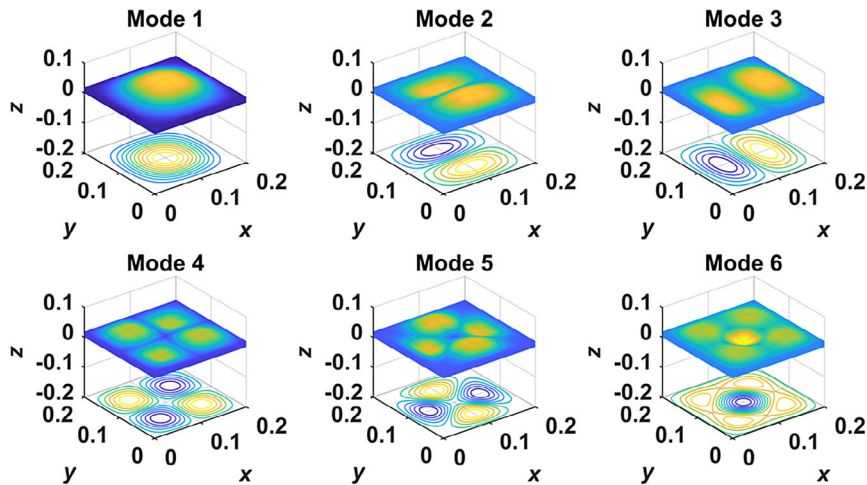
Figure 5. The first six 3D mode shapes of CCCC Al_2O_3 square plate with thickness-side ratio fixed at 0.1.

**ADVANCED
SCIENCE NEWS**
www.advancedsciencenews.com

**ADVANCED
ENGINEERING
MATERIALS**
www.aem-journal.com

3.5. Parametric Studies

Next, the validated analytical method is used to quantify the effects of plate aspect ratio a/b, volume fraction index p, and elastic restrained stiffness on the natural frequencies of $Si_3N_4/SUS304$ FG plates in different thermal environments.

Figure 6 shows the first four natural frequencies as functions of temperature for CCCC FG plates having different aspect ratios (0.5, 1.0, 1.5, and 2.0) for $a = 0.2\,m$, $h/b = 0.1$, and $p = 2$. Regardless of the plate aspect ratio, the first four natural frequencies decrease with increasing temperature: the higher the temperature, the faster the decrease. Two reasons contribute to such a variation trend: material properties vary with temperature, and thermal stresses caused by boundary conditions gradually increase with temperature. In addition, in Figure 6c, the value of λ_3 gradually approaches that of λ_4 as the temperature increases. **Figure 7** shows the vibration modes of a CCCC FG plate with a fixed aspect ratio of 1.5, at 1000 K. At 1000 K, although λ_3 and λ_4 have nearly identical values, the corresponding vibration modes are seen to be completely different. In other words, a small frequency error in thermal environments may lead to significantly mismatching mode shapes, which proves the importance of an accurate theoretical model for thermal vibration analysis.

Figure 8 shows the influence of volume fraction index on the variation of fundamental frequency with temperature for $Si_3N_4/SUS304$ FG plates. In this case, four different types of boundary condition are considered: 1) CCCC, 2) CSCS, 3) CFCF, and 4) SSSS. Intuitively, from the viewpoint of restraint stiffness, the boundary constraints weaken gradually from 1) to 2). For each type of boundary condition, a total of five FG plates with different volume fractions ($p = 0.3, 0.5, 1.0, 2.0, 10.0$) are studied. Geometric dimensions of all the FG plates remain unchanged ($a = 0.2\,m$, $a/b = 1.0$, and $h/b = 0.1$).

It can be seen from Figure 8 that the fundamental frequency of an FG plate with a large volume fraction decreases more rapidly with increasing temperature, because the larger the volume fraction, the higher the metal content. Interestingly, for a given volume fraction, when the temperature is fixed, the fundamental frequency is related to boundary condition as follows: λ (CCCC) $> \lambda$ (CSCS) $> \lambda$ (CFCF) $> \lambda$ (SSSS). This is because a weaker constraint at the edges of the FG plate decreases its flexural rigidity, resulting in lower frequency. This phenomenon is consistent with the results of Chakraverty and Pradhan for Al/Al_2O_3 FG plates with different boundary conditions.[6] For further validation, finite element (FE) analysis is also conducted to calculate the fundamental frequencies of an isotropic SUS304 plate with four different boundary conditions at 300, 500, and 700 K, respectively. **Table 3** shows the FE simulation results, which show that the variation trend of the fundamental frequency with boundary condition agrees with the present analytical result of Figure 8.
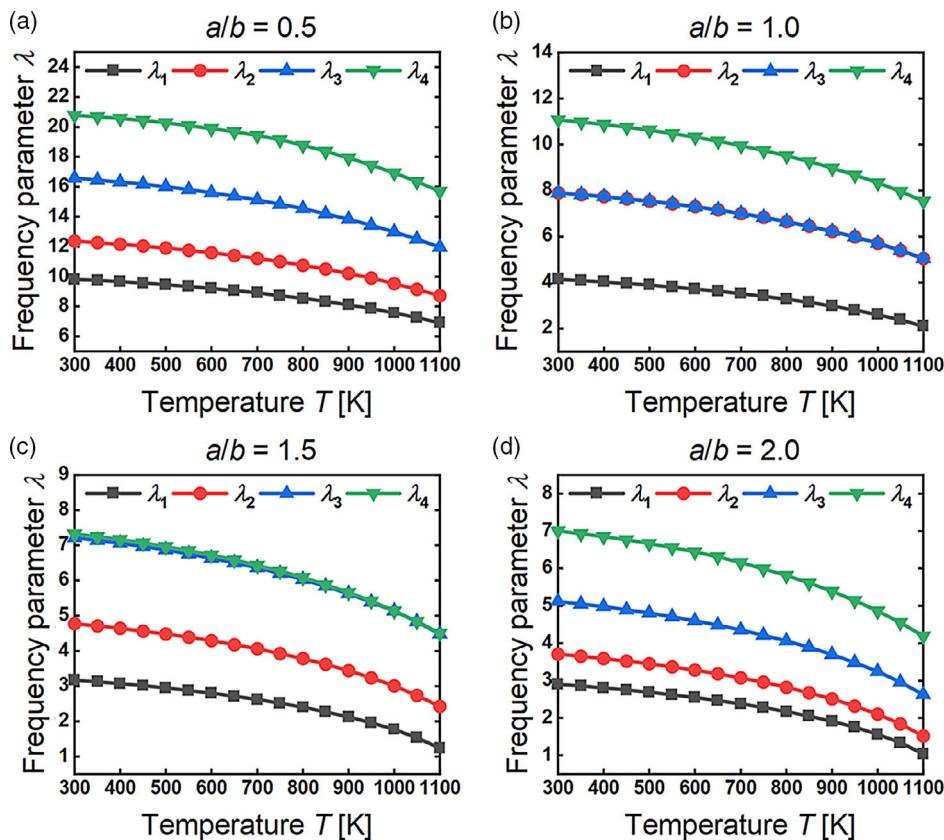
Figure 6. The first four nondimensional natural frequencies of CCCC FG plates plotted as functions of temperature ($T_0 = 300\,K$ and $300\,K \leq T \leq 1100\,K$) for selected plate aspect ratios: a) $a/b = 0.5$; b) $a/b = 1.0$; c) $a/b = 1.5$; d) $a/b = 2.0$.
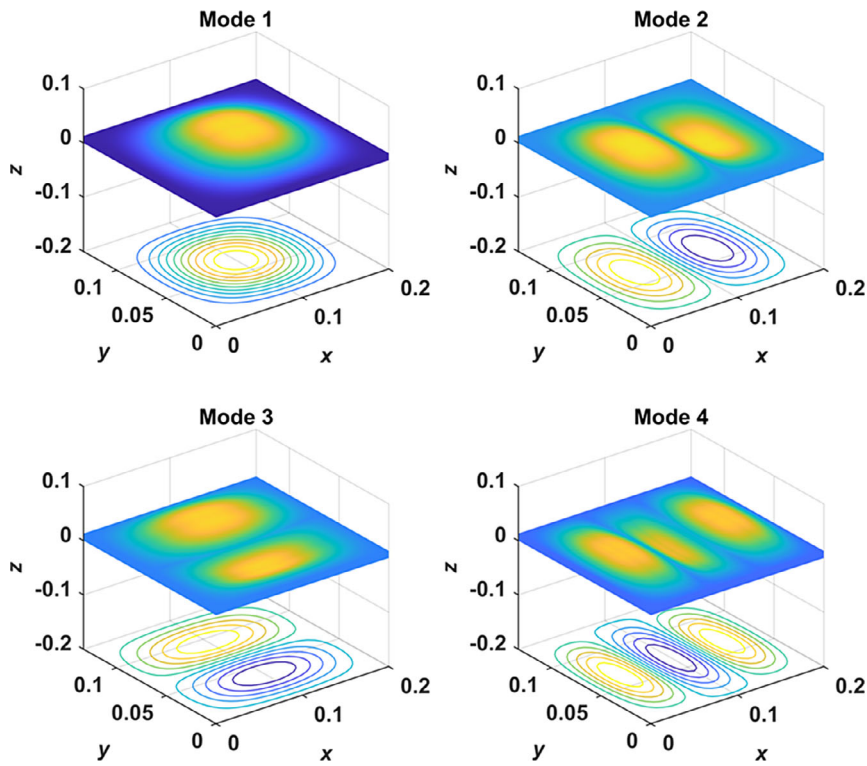
Figure 7. The first four 3D mode shapes of the CCCC FG plate with a fixed aspect ratio of 1.5 at 1000 K.
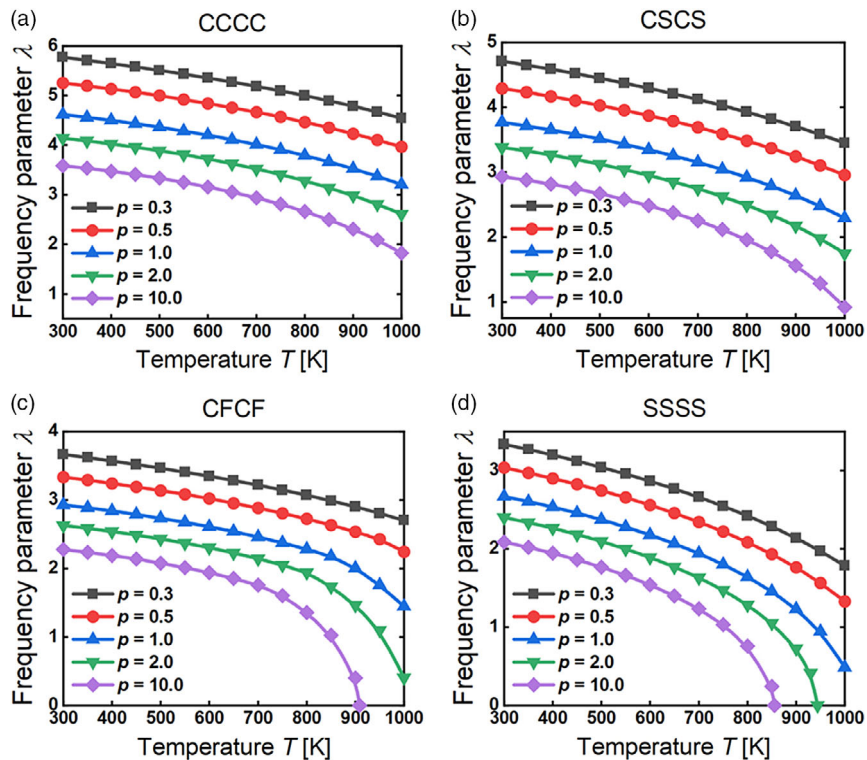
Figure 8. Fundamental frequency of Si_3N_4/SUS304 FG plate with varying volume fraction p plotted as a function of temperature ($T_0 = 300$ K and 300 K $\leq T \leq 1000$ K) for selected boundary conditions: a) CCCC; b) CSCS; c) CFCF; d) SSSS.

**ADVANCED
SCIENCE NEWS**
www.advancedsciencenews.com

**ADVANCED
ENGINEERING
MATERIALS**
www.aem-journal.com

Table 3. Fundamental frequencies of isotropic SUS304 plate with different combinations of boundary conditions in thermal environments ($a = 0.2$ m, $a/b = 1.0$, $h/b = 0.1$).

Temperature T [K]	Fundamental frequency [Hz]			
	CCCC	CSCS	CFCF	SSSS
300	4009.0	3280.5	2539.6	2331.2
500	3777.7	3124.8	2363.6	2215.9
700	3449.2	2894.2	2187.8	2049.1

The fundamental frequency of an FG plate with a fixed volume fraction of 10 drops to zero at the critical temperature of 908.5 K (CFCF plate), as shown in Figure 8c, and 855.6 K (SSSS plate), as shown in Figure 8d. In particular, the fundamental frequency of an FG plate with a fixed volume fraction of 2 drops to zero at the critical temperature of 944.0 K in Figure 8d. Physically, according to Chen et al.,[36] such an FG plate will buckle when its fundamental frequency drops to zero. Given that the boundary conditions in Figure 8a,d are CCCC and SSSS, respectively, it can be inferred that an FG plate with weaker boundary constraints is more prone to buckling in thermal environments. In other words, the present analytical method not only can

predict the buckling of an FG plate but also can accurately determine its critical buckling temperature.

Figure 9 and **10** show how the fundamental frequency of Si_3N_4/SUS304 FG plate varies with the spring stiffness of elastic boundaries at different temperature rises: 100, 300, and 500 K. For the plotting, relevant parameters are fixed at: $a = 0.2$ m, $a/b = 1.0$, $h/b = 0.1$, and $p = 1$.

Specifically, the four boundary conditions in Figure 9 contain the combination of simply supported boundary (S) and elastic constraints approaching the simply supported form (E_s). From Figure 9a–d, in terms of spring stiffness, the elastic boundaries of the FG plate gradually vary, as follows (in abbreviation): a) $SSSE_s$; b) SSE_sE_s; c) $SE_sE_sE_s$; and d) $E_sE_sE_sE_s$.

In Figure 10, the four boundary condition types are composed of clamped boundary (C) and elastic constraints approaching the clamped form (E_c). From Figure 10a–d, the order of change in elastic boundaries is similar to Figure 9, as a) $CCCE_c$; b) CCE_cE_c; c) $CE_cE_cE_c$; and d) $E_cE_cE_cE_c$.

Table 4 shows the spring stiffness values of elastic boundaries adopted to construct Figure 9 and 10.

The results of Figure 9 and 10 reveal some new phenomena of natural frequency varying with elastic boundary conditions in different thermal environments. In Figure 9, when the stiffness of elastic boundary decreases, the (nondimensional) fundamental
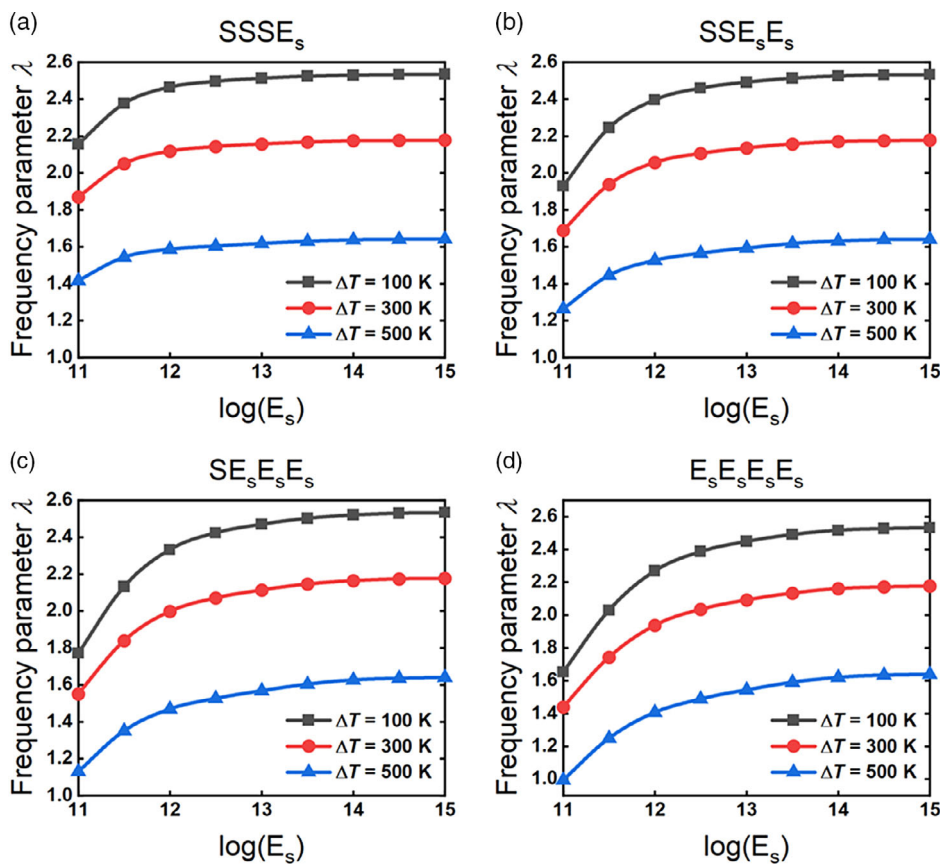
Figure 9. Nondimensional fundamental frequency λ of Si_3N_4/SUS304 FG plate plotted as a function of spring stiffness at different temperature rises ($\Delta T = T - T_0$ and $T_0 = 300$ K) for elastic constraints in simply supported form: a) $SSSE_s$; b) SSE_sE_s; c) $SE_sE_sE_s$; d) $E_sE_sE_sE_s$.

**ADVANCED
SCIENCE NEWS**

www.advancedsciencenews.com

**ADVANCED
ENGINEERING
MATERIALS**

www.aem-journal.com
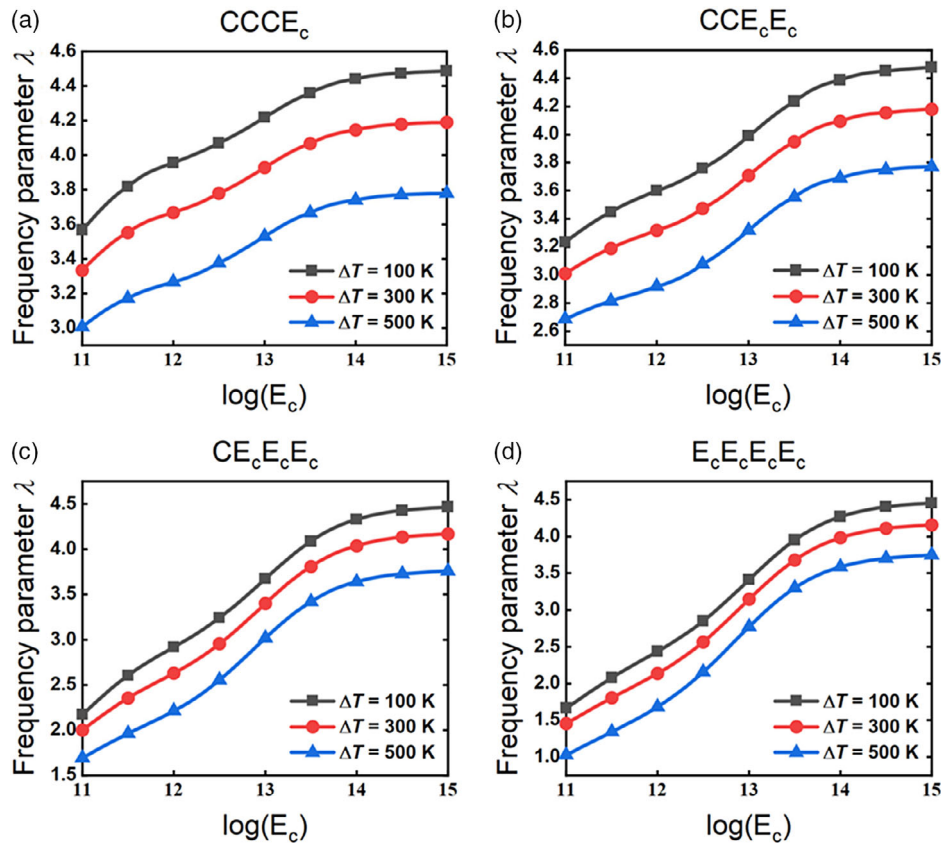
Figure 10. Nondimensional fundamental frequency λ of Si_3N_4/SUS304 FG plate plotted as a function of spring stiffness at different temperature rises ($\Delta T = T - T_0$ and $T_0 = 300$ K) for elastic constraints in clamped form: a) $CCCE_c$; b) CCE_cE_c; c) $CE_cE_cE_c$; d) $E_cE_cE_cE_c$.

Table 4. Spring stiffness values for two different types of elastic constraint boundary conditions.

Edge	Stiffness of elastic boundaries	
	E_s [N/m]	E_c [N/m]
$x = 0$	$ku = 0$, $kv = kw = $1e-11−1e-15	$ku = kv = kw = $1e-11−1e-15
$x = a$	$ku = 0$, $kv = kw = $1e-11−1e-15	$ku = kv = kw = $1e-11−1e-15
$y = 0$	$kv = 0$, $ku = kw = $1e-11−1e-15	$ku = kv = kw = $1e-11−1e-15
$y = b$	$kv = 0$, $ku = kw = $1e-11−1e-15	$ku = kv = kw = $1e-11−1e-15

frequency of an FG plate decreases continuously: the smaller the stiffness, the faster the fundamental frequency decreases. Meanwhile, the more the edges are elastically constrained, the more the fundamental frequency decreases. When the stiffness of elastic boundaries is increased from 1e-11 to 1e-15, the higher the temperature, the more the fundamental frequency decreases. As for Figure 10, although the fundamental frequency decreases with decreasing boundary stiffness, the downtrend slightly increases and then decreases. As the number of elastic boundaries increases, the extent to which the fundamental frequency decreases is enlarged. The influence of temperature on the variation of the fundamental frequency is similar to that shown in Figure 9.

4. Conclusion

Based on the theory of 3D elasticity, an analytical method has been developed to predict the free vibration performance of an FG rectangular plate with arbitrary boundary conditions in thermal environments. The convergence and accuracy of the proposed method are validated against existing analytical results for both isotropic and FG plates, with excellent agreement achieved. The method is then utilized to conduct a systematic parameter analysis to highlight the effects of plate aspect ratio, volume fraction, and elastic boundary on the free vibration characteristics of the FG plate set in different temperatures. No matter how its aspect ratio changes, the natural frequency of the FG plate decreases with increasing temperature. When the boundary constraint is relatively weak, the natural frequency drops to zero at a critical temperature, that is, the critical buckling temperature. With elastic boundary conditions considered, the sensitivity of natural frequency to spring stiffness increases with the number of elastic edges. The proposed analytical method can be readily extended to deal with more complicated situations, like nonuniform elastic restraint of plate edges and nonuniform and/or transient temperature rises, which are important for designing supersonic aircraft. In addition, the current work can be extended to study the free vibration of FG smart materials, such as FG electro- and FG magnetoactive materials,[2,3] by developing relevant constitutive relations on the basis of nonlinear thermo–electric–elasticity and thermo–magnetic–elasticity.

Appendix A. Supplementary Tables

Table A.1. Temperature-dependent coefficients of Young's modulus E, Poisson ratio ν, and thermal expansion coefficient α of Si_3N_4 and SUS304.[32]

Material	Properties	P_{-1}	P_0	P_1	P_2	P_3	P (300 K)
Si_3N_4	E [Pa]	0	348.43e-9	−3.070e-4	2.160e-7	−8.946e-11	322.2715e-9
	ν	0	0.2400	0	0	0	0.2400
	α [1/K]	0	5.8723e-6	9.095e-4	0	0	7.4746e-6
	ρ [kg m^{-3}]	0	2370	0	0	0	2370
SUS304	E [Pa]	0	201.04e-9	3.079e-4	−6.534e-7	0	207.7877e-9
	ν	0	0.3262	−2.002e-4	3.797e-7	0	0.3178
	α [1/K]	0	12.330e-6	8.086e-4	0	0	1.5321e-5
	ρ [kg m^{-3}]	0	8166	0	0	0	8166

Table A.2. Spring stiffness setup for classical boundary conditions.

Edge	Boundary condition	Spring stiffness [N/m]		
		ku	kv	kw
$x = 0$	Free (F)	0	0	0
	Simply supported (S)	0	1e-19	1e-19
	Clamped (C)	1e-19	1e-19	1e-19
$x = a$	Free (F)	0	0	0
	Simply supported (S)	0	1e-19	1e-19
	Clamped (C)	1e-19	1e-19	1e-19
$y = 0$	Free (F)	0	0	0
	Simply supported (S)	1e-19	0	1e-19
	Clamped (C)	1e-19	1e-19	1e-19
$y = b$	Free (F)	0	0	0
	Simply supported (S)	1e-19	0	1e-19
	Clamped (C)	1e-19	1e-19	1e-19

Table A.3. The first seven frequency parameters for isotropic Al_2O_3 square plates ($T_0 = 300$ K) for selected boundary conditions: comparison between the present analytical method and those in the open literature.

Case	h/b	Source	Frequency parameters						
			θ_1	θ_2	θ_3	θ_4	θ_5	θ_6	θ_7
SSSS	0.1	Jin[28]	19.098	45.636	45.636	64.384	64.384	70.149	85.500
		Liew[33]	19.090	45.619	45.619	64.383	64.383	70.104	85.488
		present	19.100	45.639	45.639	64.384	64.384	70.156	85.503
	0.2	Jin[28]	17.528	32.192	32.192	38.488	38.488	45.526	55.802
		Liew[33]	17.526	32.192	32.192	38.483	38.483	45.526	55.787
		present	17.529	32.192	32.192	32.489	32.489	45.526	55.804
	0.5	Jin[28]	12.426	12.877	12.877	18.210	23.009	23.009	25.753
		Liew[33]	12.426	12.877	12.877	18.210	23.007	23.007	25.753
		present	12.426	12.877	12.877	18.210	23.010	23.010	25.753

**ADVANCED
SCIENCE NEWS**

www.advancedsciencenews.com

**ADVANCED
ENGINEERING
MATERIALS**

www.aem-journal.com

Table A.3. Continued.

Case	h/b	Source	Frequency parameters						
			θ_1	θ_2	θ_3	θ_4	θ_5	θ_6	θ_7
CCCC	0.1	Jin[28]	33.009	63.043	63.043	88.411	104.28	105.29	123.73
		Liew[33]	32.782	62.630	62.630	87.896	103.61	104.60	123.59
		present	33.032	63.102	63.102	88.496	104.37	105.39	123.74
	0.2	Jin[28]	27.065	47.346	47.346	62.000	62.000	63.635	72.604
		Liew[33]	26.906	47.103	47.103	61.917	61.917	63.348	72.286
		present	27.081	47.386	47.386	62.009	62.009	63.688	72.657
	0.5	Jin[28]	15.358	24.136	24.136	24.866	24.866	29.379	31.578
		Liew[33]	15.294	24.078	24.078	24.832	24.832	29.377	31.210
		present	15.366	24.148	24.148	24.869	24.869	29.379	31.594
FFFF	0.1	Jin[28]	12.728	18.956	23.346	31.965	31.965	55.493	55.493
		Liew[34]	12.726	18.955	23.347	31.965	31.965	55.493	55.493
		present	12.730	18.958	23.348	31.967	31.967	55.454	55.454
	0.2	Jin[28]	11.710	17.433	21.252	27.648	27.648	40.192	42.775
		Liew[34]	11.710	17.433	21.252	27.647	27.647	40.191	42.776
		present	11.711	17.434	21.253	27.659	27.649	40.192	42.775
	0.5	Jin[28]	8.7801	12.515	14.962	16.072	17.030	17.030	17.632
		Liew[34]	8.7802	12.515	14.962	16.073	17.030	17.030	17.631
		present	8.7802	12.515	14.962	16.072	17.030	17.030	17.632

Table A.4. Nondimensional natural frequency λ for CCCC square Si_3N_4/SUS304 FG plates subjected to different temperature rises ($T_0 = 300$ K, $\Delta T = T - T_0$): comparison between the present analytical method and those in the existing literature.

ΔT [K]	Source	Natural frequency							
		λ_1	λ_2	λ_3	λ_4	λ_5	λ_6	λ_7	λ_8
0	Yang[14]	4.1062	7.8902	7.8902	11.1834	12.5881	13.1867	15.4530	16.0017
	Li[17]	4.1658	7.9389	7.9389	11.1212	13.0973	13.2234	15.3627	15.3627
	Kim[35]	4.1165	7.9696	7.9696	11.2198	13.1060	13.2089	15.9471	15.9471
	present	4.1389	7.9011	7.9011	11.0783	13.0550	13.1824	15.4525	15.4525
300	Yang[14]	3.6636	7.2544	7.2544	10.3924	11.7054	12.3175	14.4520	15.0019
	Li[17]	3.7202	7.3010	7.3010	10.3348	12.2256	12.3563	14.8112	14.8112
	Kim[35]	3.6593	7.3098	7.3098	10.4021	12.1928	12.3052	14.9090	14.9090
	present	3.7222	7.2953	7.2953	10.3251	12.2168	12.3481	14.8106	14.8106
500	Yang[14]	3.2357	6.6281	6.6281	9.5900	10.8285	11.4350	13.4412	13.9756
	Li[17]	3.2747	6.6509	6.6509	9.5192	11.3126	11.4468	13.7907	13.7907
	Kim[35]	3.2147	6.6561	6.6561	9.5761	11.2708	11.3812	13.8346	13.8346
	present	3.2811	6.6511	6.6511	9.5157	11.3099	11.4455	13.7863	13.7863

Table A.5. Nondimensional natural frequency λ for CCCC rectangular Si_3N_4/SUS304 FG plates with different aspect ratios a/b and different volume fraction index p subjected to uniform temperature rise ($T_0 = 300$ K, $\Delta T = T - T_0 = 300$ K): comparison between the present analytical method and those in the existing literature.

p	a/b	Source	Natural frequency						
			λ_1	λ_2	λ_3	λ_4	λ_5	λ_6	λ_7
2	0.5	Yang[14]	9.2196	11.6913	15.2957	20.4667	21.2323	21.4468	22.4853
		Li[17]	9.2111	11.5890	15.5999	19.9043	20.0234	20.7922	21.9073
		present	9.2051	11.5831	15.5976	19.8983	20.0595	20.8200	21.9454

**ADVANCED
SCIENCE NEWS**

www.advancedsciencenews.com

**ADVANCED
ENGINEERING
MATERIALS**

www.aem-journal.com

Table A.5. Continued.

p	a/b	Source	Natural frequency						
			λ_1	λ_2	λ_3	λ_4	λ_5	λ_6	λ_7
	1.0	Yang[14]	3.6636	7.2544	7.2544	10.3924	11.7054	12.3175	14.4520
		Li[17]	3.7202	7.3010	7.3010	10.3348	12.2256	12.3563	14.8112
		present	3.7222	7.2953	7.2953	10.3251	12.2168	12.3481	14.8106
	1.5	Yang[14]	2.7373	4.2236	6.6331	6.6331	7.9088	9.8122	10.0191
		Li[17]	2.7904	4.2839	6.6401	6.7227	7.8941	9.8528	9.9676
		present	2.7976	4.2890	6.6367	6.7201	7.8889	9.8492	9.9585
10	0.5	Yang[14]	7.9839	10.1219	13.3088	17.6295	18.3727	18.9066	19.3778
		Li[17]	7.8170	9.8332	13.2410	16.8733	16.9943	17.6538	18.5960
		present	7.8392	9.8607	13.2733	16.8710	17.0290	17.6972	18.6311
	1.0	Yang[14]	3.1835	6.3001	6.3001	9.0171	10.2372	10.6781	12.6015
		Li[17]	3.1398	6.1857	6.1857	8.7653	10.3727	10.4866	12.5971
		present	3.1567	6.2123	6.2123	8.7971	10.4054	10.5216	12.6226
	1.5	Yang[14]	2.3753	3.6692	5.7618	5.7618	6.8690	8.5206	8.6979
		Li[17]	2.3470	3.6147	5.6234	5.6910	6.6888	8.3553	8.4522
		present	2.3620	3.6365	5.6495	5.7198	6.7185	8.3957	8.4845

Appendix B. Detailed Expression of Matrices in Theoretical Formulas

With reference to Equation (29), to clearly show each element in a matrix, the indices of the matrix are given as

$$i = l \cdot M \cdot N + n \cdot M + m + 1 \tag{B.1}$$

$$j = o \cdot M \cdot N + q \cdot M + p + 1 \tag{B.2}$$

$$i1 = (r-1) \cdot M \cdot N + n \cdot M + m + 1 \tag{B.3}$$

$$j1 = (s-1) \cdot M \cdot N + q \cdot M + p + 1 \tag{B.4}$$

$$i2 = (r-1) \cdot M \cdot L + l \cdot M + m + 1 \tag{B.5}$$

$$j2 = (s-1) \cdot M \cdot L + o \cdot M + p + 1 \tag{B.6}$$

$$i3 = (r-1) \cdot N \cdot L + l \cdot N + n + 1 \tag{B.7}$$

$$j3 = (s-1) \cdot N \cdot L + o \cdot N + q + 1 \tag{B.8}$$

where $m = 0, 1, ..., M-1$; $p = 0, 1, ..., M-1$; $n = 0, 1, ..., N-1$; $q = 0, 1, ..., N-1$; $l = 0, 1, ..., L-1$; $o = 0, 1, ..., L-1$; $r = 1, 2$; and $s = 1, 2$.

For stiffness matrix $[K]$, detailed expressions of its first row are

$$[K_{1,1}]_{i,j} = X_{cc}^{11}Y_{cc}^{00}A\_Z_{cc}^{00} + X_{cc}^{00}Y_{cc}^{11}C\_Z_{cc}^{00} + X_{cc}^{00}Y_{cc}^{00}C\_Z_{cc}^{11} \tag{B.9}$$

$$[K_{1,2}]_{i,j1} = X_{cc}^{11}Y_{cc}^{00}A\_Z_{c\xi}^{00} + X_{cc}^{00}Y_{cc}^{11}C\_Z_{c\xi}^{00} + X_{cc}^{00}Y_{cc}^{00}C\_Z_{c\xi}^{11} \tag{B.10}$$

$$[K_{1,3}]_{i,j2} = X_{cc}^{11}Y_{c\xi}^{00}A\_Z_{cc}^{00} + X_{cc}^{00}Y_{c\xi}^{11}C\_Z_{cc}^{00} + X_{cc}^{00}Y_{c\xi}^{00}C\_Z_{cc}^{11} \tag{B.11}$$

$$[K_{1,4}]_{i,j3} = X_{c\xi}^{11}Y_{cc}^{00}A\_Z_{cc}^{00} + X_{c\xi}^{00}Y_{cc}^{11}C\_Z_{cc}^{00} + X_{c\xi}^{00}Y_{cc}^{00}C\_Z_{cc}^{11} \tag{B.12}$$

$$[K_{1,5}]_{i,j} = X_{cc}^{10}Y_{cc}^{01}B\_Z_{cc}^{00} + X_{cc}^{01}Y_{cc}^{10}C\_Z_{cc}^{00} \tag{B.13}$$

$$[K_{1,6}]_{i,j1} = X_{cc}^{10}Y_{cc}^{01}B\_Z_{c\xi}^{00} + X_{cc}^{01}Y_{cc}^{10}C\_Z_{c\xi}^{00} \tag{B.14}$$

$$[K_{1,7}]_{i,j2} = X_{cc}^{10}Y_{c\xi}^{01}B\_Z_{cc}^{00} + X_{cc}^{01}Y_{c\xi}^{10}C\_Z_{cc}^{00} \tag{B.15}$$

$$[K_{1,8}]_{i,j3} = X_{c\xi}^{10}Y_{cc}^{01}B\_Z_{cc}^{00} + X_{c\xi}^{01}Y_{cc}^{10}C\_Z_{cc}^{00} \tag{B.16}$$

$$[K_{1,9}]_{i,j} = X_{cc}^{10}Y_{cc}^{01}B\_Z_{cc}^{00} + X_{cc}^{01}Y_{cc}^{00}C\_Z_{cc}^{01} \tag{B.17}$$

$$[K_{1,10}]_{i,j1} = X_{cc}^{10}Y_{cc}^{01}B\_Z_{c\xi}^{00} + X_{cc}^{01}Y_{cc}^{00}C\_Z_{c\xi}^{01} \tag{B.18}$$

$$[K_{1,11}]_{i,j2} = X_{cc}^{10}Y_{c\xi}^{01}B\_Z_{cc}^{00} + X_{cc}^{01}Y_{c\xi}^{00}C\_Z_{cc}^{01} \tag{B.19}$$

$$[K_{1,12}]_{i,j3} = X_{c\xi}^{10}Y_{cc}^{01}B\_Z_{cc}^{00} + X_{c\xi}^{01}Y_{cc}^{00}C\_Z_{cc}^{01} \tag{B.20}$$

Detailed expressions of stiffness matrix $[K_s]$ are

$$[K_s] = \begin{bmatrix} [K^s]_{uu} & 0 & 0 \\ 0 & [K^s]_{vv} & 0 \\ 0 & 0 & [K^s]_{ww} \end{bmatrix} \tag{B.21}$$

$$[K^s]_{uu} = \begin{bmatrix} [K_{1,1}^s] & [K_{1,2}^s] & [K_{1,3}^s] & [K_{1,4}^s] \\ & [K_{2,2}^s] & [K_{2,3}^s] & [K_{2,4}^s] \\ & & [K_{3,3}^s] & [K_{3,4}^s] \\ \text{sym} & & & [K_{4,4}^s] \end{bmatrix} \tag{B.22}$$

$$[K_{1,1}^s]_{i,j} = ku_{x0}Y_{cc}^{00}Z_{cc}^{00} + ku_{xa}(-1)^{m+p}Y_{cc}^{00}Z_{cc}^{00} + ku_{y0}X_{cc}^{00}Z_{cc}^{00} + ku_{yb}(-1)^{n+q}X_{cc}^{00}Z_{cc}^{00} \tag{B.23}$$

$$[K_{1,2}^s]_{i,j1} = ku_{x0}Y_{cc}^{00}Z_{c\xi}^{00} + ku_{xa}(-1)^{m+p}Y_{cc}^{00}Z_{c\xi}^{00} + ku_{y0}X_{cc}^{00}Z_{c\xi}^{00} + ku_{yb}(-1)^{n+q}X_{cc}^{00}Z_{c\xi}^{00} \tag{B.24}$$

$$[K_{1,3}^s]_{i,j2} = ku_{x0}Y_{c\xi}^{00}Z_{cc}^{00} + ku_{xa}(-1)^{m+p}Y_{c\xi}^{00}Z_{cc}^{00} \tag{B.25}$$

$$[K_{1,4}^s]_{i,j3} = ku_{y0}X_{c\xi}^{00}Z_{cc}^{00} + ku_{yb}(-1)^{n+q}X_{c\xi}^{00}Z_{cc}^{00} \tag{B.26}$$

$$[K_{2,2}^s]_{i1,j1} = ku_{x0}Y_{cc}^{00}Z_{\xi\xi}^{00} + ku_{xa}(-1)^{m+p}Y_{cc}^{00}Z_{\xi\xi}^{00} + ku_{y0}X_{cc}^{00}Z_{\xi\xi}^{00} + ku_{yb}(-1)^{n+q}X_{cc}^{00}Z_{\xi\xi}^{00} \tag{B.27}$$

$$[K^s_{2,3}]_{i1,j2} = ku_{x0}Y^{00}_{c\xi}Z^{00}_{\xi c} + ku_{xa}(-1)^{m+p}Y^{00}_{c\xi}Z^{00}_{\xi c} \tag{B.28}$$

$$[K^s_{2,4}]_{i1,j3} = ku_{y0}X^{00}_{c\xi}Z^{00}_{\xi c} + ku_{yb}(-1)^{n+q}X^{00}_{c\xi}Z^{00}_{\xi c} \tag{B.29}$$

$$[K^s_{3,3}]_{i2,j2} = ku_{x0}Y^{00}_{\xi\xi}Z^{00}_{cc} + ku_{xa}(-1)^{m+p}Y^{00}_{\xi\xi}Z^{00}_{cc} \tag{B.30}$$

$$[K^s_{3,4}]_{i2,j3} = 0 \tag{B.31}$$

$$[K^s_{4,4}]_{i3,j3} = ku_{y0}X^{00}_{\xi\xi}Z^{00}_{cc} + ku_{yb}(-1)^{n+q}X^{00}_{\xi\xi}Z^{00}_{cc} \tag{B.32}$$

where the matrices $[K^s]_{vv}$ and $[K^s]_{ww}$ can be easily obtained by replacing the spring stiffness ku in the matrix $[K^s]_{uu}$ with kv and kw, respectively.

Detailed expressions of stiffness matrix $[K_T]$ are

$$[K_T] = \begin{bmatrix} [K^T]_{uu} & 0 & 0 \\ 0 & [K^T]_{vv} & 0 \\ 0 & 0 & [K^T]_{ww} \end{bmatrix} \tag{B.33}$$

$$[K^T]_{uu} = [K^T]_{vv} = [K^T]_{ww} = \begin{bmatrix} [K^T_{1,1}] & [K^T_{1,2}] & [K^T_{1,3}] & [K^T_{1,4}] \\ & [K^T_{2,2}] & [K^T_{2,3}] & [K^T_{2,4}] \\ & & [K^T_{3,3}] & [K^T_{3,4}] \\ \text{sym} & & & [K^T_{4,4}] \end{bmatrix} \tag{B.34}$$

$$[K^T_{1,1}]_{i,j} = (X^{11}_{cc}Y^{00}_{cc}T\_Z^{00}_{cc} + X^{00}_{cc}Y^{11}_{cc}T\_Z^{00}_{cc})\Delta T \tag{B.35}$$

$$[K^T_{1,2}]_{i,j1} = (X^{11}_{cc}Y^{00}_{cc}T\_Z^{00}_{c\xi} + X^{00}_{cc}Y^{11}_{cc}T\_Z^{00}_{c\xi})\Delta T \tag{B.36}$$

$$[K^T_{1,3}]_{i,j2} = (X^{11}_{cc}Y^{00}_{c\xi}T\_Z^{00}_{cc} + X^{00}_{cc}Y^{11}_{c\xi}T\_Z^{00}_{cc})\Delta T \tag{B.37}$$

$$[K^T_{1,4}]_{i,j3} = (X^{11}_{c\xi}Y^{00}_{cc}T\_Z^{00}_{cc} + X^{00}_{c\xi}Y^{11}_{cc}T\_Z^{00}_{cc})\Delta T \tag{B.38}$$

$$[K^T_{2,2}]_{i1,j1} = (X^{11}_{cc}Y^{00}_{cc}T\_Z^{00}_{\xi\xi} + X^{00}_{cc}Y^{11}_{cc}T\_Z^{00}_{\xi\xi})\Delta T \tag{B.39}$$

$$[K^T_{2,3}]_{i1,j2} = (X^{11}_{cc}Y^{00}_{c\xi}T\_Z^{00}_{\xi c} + X^{00}_{cc}Y^{11}_{c\xi}T\_Z^{00}_{\xi c})\Delta T \tag{B.40}$$

$$[K^T_{2,4}]_{i1,j3} = (X^{11}_{c\xi}Y^{00}_{cc}T\_Z^{00}_{\xi c} + X^{00}_{c\xi}Y^{11}_{cc}T\_Z^{00}_{\xi c})\Delta T \tag{B.41}$$

$$[K^T_{3,3}]_{i2,j2} = (X^{11}_{cc}Y^{00}_{\xi\xi}T\_Z^{00}_{cc} + X^{00}_{cc}Y^{11}_{\xi\xi}T\_Z^{00}_{cc})\Delta T \tag{B.42}$$

$$[K^T_{3,4}]_{i2,j3} = (X^{11}_{c\xi}Y^{00}_{\xi c}T\_Z^{00}_{cc} + X^{00}_{c\xi}Y^{11}_{\xi c}T\_Z^{00}_{cc})\Delta T \tag{B.43}$$

$$[K^T_{4,4}]_{i3,j3} = (X^{11}_{\xi\xi}Y^{00}_{cc}T\_Z^{00}_{cc} + X^{00}_{\xi\xi}Y^{11}_{cc}T\_Z^{00}_{cc})\Delta T \tag{B.44}$$

Detailed expressions of mass matrix $[M]$ are

$$[M] = \begin{bmatrix} [M]_{uu} & 0 & 0 \\ 0 & [M]_{vv} & 0 \\ 0 & 0 & [M]_{ww} \end{bmatrix} \tag{B.45}$$

$$[M]_{uu} = [M]_{vv} = [M]_{ww} = \begin{bmatrix} [M_{1,1}] & [M_{1,2}] & [M_{1,3}] & [M_{1,4}] \\ & [M_{2,2}] & [M_{2,3}] & [M_{2,4}] \\ & & [M_{3,3}] & [M_{3,4}] \\ \text{sym} & & & [M_{4,4}] \end{bmatrix} \tag{B.46}$$

$$[M_{1,1}]_{i,j} = X^{00}_{cc}Y^{00}_{cc}\rho\_Z^{00}_{cc} \tag{B.47}$$

$$[M_{1,2}]_{i,j1} = X^{00}_{cc}Y^{00}_{cc}\rho\_Z^{00}_{c\xi} \tag{B.48}$$

$$[M_{1,3}]_{i,j2} = X^{00}_{cc}Y^{00}_{c\xi}\rho\_Z^{00}_{cc} \tag{B.49}$$

$$[M_{1,4}]_{i,j3} = X^{00}_{c\xi}Y^{00}_{cc}\rho\_Z^{00}_{cc} \tag{B.50}$$

$$[M_{2,2}]_{i1,j1} = X^{00}_{cc}Y^{00}_{cc}\rho\_Z^{00}_{\xi\xi} \tag{B.51}$$

$$[M_{2,3}]_{i1,j2} = X^{00}_{cc}Y^{00}_{c\xi}\rho\_Z^{00}_{\xi c} \tag{B.52}$$

$$[M_{2,4}]_{i1,j3} = X^{00}_{c\xi}Y^{00}_{cc}\rho\_Z^{00}_{\xi c} \tag{B.53}$$

$$[M_{3,3}]_{i2,j2} = X^{00}_{cc}Y^{00}_{\xi\xi}\rho\_Z^{00}_{cc} \tag{B.54}$$

$$[M_{3,4}]_{i2,j3} = X^{00}_{c\xi}Y^{00}_{\xi c}\rho\_Z^{00}_{cc} \tag{B.55}$$

$$[M_{4,4}]_{i3,j3} = X^{00}_{\xi\xi}Y^{00}_{cc}\rho\_Z^{00}_{cc} \tag{B.56}$$

Detailed expressions of integral operations are

$$X^{ef}_{cc} = \int_0^a \frac{d^e\cos(\lambda_m x)}{dx^e}\frac{d^f\cos(\lambda_p x)}{dx^f}dx$$

$$X^{ef}_{\xi c} = \int_0^a \frac{d^e\xi_t(x)}{dx^e}\frac{d^f\cos(\lambda_p x)}{dx^f}dx \tag{B.57-58}$$

$$X^{ef}_{c\xi} = \int_0^a \frac{d^e\cos(\lambda_m x)}{dx^e}\frac{d^f\xi_k(x)}{dx^f}dx$$

$$X^{ef}_{\xi\xi} = \int_0^a \frac{d^e\xi_t(x)}{dx^e}\frac{d^f\xi_k(x)}{dx^f}dx \tag{B.59-60}$$

$$Y^{ef}_{cc} = \int_0^b \frac{d^e\cos(\lambda_n\gamma)}{d\gamma^e}\frac{d^f\cos(\lambda_q\gamma)}{d\gamma^f}d\gamma$$

$$Y^{ef}_{\xi c} = \int_0^b \frac{d^e\xi_t(x)}{d\gamma^e}\frac{d^f\cos(\lambda_p x)}{d\gamma^f}d\gamma \tag{B.61-62}$$

$$Y^{ef}_{c\xi} = \int_0^b \frac{d^e\cos(\lambda_n\gamma)}{d\gamma^e}\frac{d^f\xi_k(\gamma)}{d\gamma^f}d\gamma$$

$$Y^{ef}_{\xi\xi} = \int_0^b \frac{d^e\xi_t(\gamma)}{d\gamma^e}\frac{d^f\xi_k(\gamma)}{d\gamma^f}d\gamma \tag{B.63-64}$$

$$Z^{ef}_{cc} = \int_0^h \frac{d^e\cos(\lambda_l z)}{dz^e}\frac{d^f\cos(\lambda_o z)}{dz^f}dz$$

$$Z^{ef}_{\xi c} = \int_0^h \frac{d^e\xi_t(z)}{dz^e}\frac{d^f\cos(\lambda_o z)}{dz^f}dz \tag{B.65-66}$$

$$Z^{ef}_{c\xi} = \int_0^h \frac{d^e\cos(\lambda_l z)}{dz^e}\frac{d^f\xi_k(z)}{dz^f}dz$$

$$Z^{ef}_{\xi\xi} = \int_0^h \frac{d^e\xi_t(z)}{dz^e}\frac{d^f\xi_k(z)}{dz^f}dz \tag{B.67-68}$$

$$A\_Z^{ef}_{cc} = \int_0^h A\frac{d^e\cos(\lambda_l z)}{dz^e}\frac{d^f\cos(\lambda_o z)}{dz^f}dz$$

$$A\_Z^{ef}_{\xi c} = \int_0^h A\frac{d^e\xi_t(z)}{dz^e}\frac{d^f\cos(\lambda_o z)}{dz^f}dz \tag{B.69-70}$$

$$A\_Z^{ef}_{c\xi} = \int_0^h A\frac{d^e\cos(\lambda_l z)}{dz^e}\frac{d^f\xi_k(z)}{dz^f}dz$$

$$A\_Z^{ef}_{\xi\xi} = \int_0^h A\frac{d^e\xi_t(z)}{dz^e}\frac{d^f\xi_k(z)}{dz^f}dz \tag{B.71-72}$$

$$B\_Z_{cc}^{ef} = \int_0^h B \frac{d^e \cos(\lambda_l z)}{dz^e} \frac{d^f \cos(\lambda_o z)}{dz^f} dz \qquad \text{(B.73-74)}$$

$$B\_Z_{\xi c}^{ef} = \int_0^h B \frac{d^e \xi_t(z)}{dz^e} \frac{d^f \cos(\lambda_o z)}{dz^f} dz$$

$$B\_Z_{c\xi}^{ef} = \int_0^h B \frac{d^e \cos(\lambda_l z)}{dz^e} \frac{d^f \xi_k(z)}{dz^f} dz \qquad \text{(B.75-76)}$$

$$B\_Z_{\xi\xi}^{ef} = \int_0^h B \frac{d^e \xi_t(z)}{dz^e} \frac{d^f \xi_k(z)}{dz^f} dz$$

$$C\_Z_{cc}^{ef} = \int_0^h C \frac{d^e \cos(\lambda_l z)}{dz^e} \frac{d^f \cos(\lambda_o z)}{dz^f} dz \qquad \text{(B.77-78)}$$

$$C\_Z_{\xi c}^{ef} = \int_0^h C \frac{d^e \xi_t(z)}{dz^e} \frac{d^f \cos(\lambda_o z)}{dz^f} dz$$

$$C\_Z_{c\xi}^{ef} = \int_0^h C \frac{d^e \cos(\lambda_l z)}{dz^e} \frac{d^f \xi_k(z)}{dz^f} dz \qquad \text{(B.79-80)}$$

$$C\_Z_{\xi\xi}^{ef} = \int_0^h C \frac{d^e \xi_t(z)}{dz^e} \frac{d^f \xi_k(z)}{dz^f} dz$$

$$\rho\_Z_{cc}^{ef} = \int_0^h \rho(z) \frac{d^e \cos(\lambda_l z)}{dz^e} \frac{d^f \cos(\lambda_o z)}{dz^f} dz \qquad \text{(B.81-82)}$$

$$\rho\_Z_{\xi c}^{ef} = \int_0^h \rho(z) \frac{d^e \xi_t(z)}{dz^e} \frac{d^f \cos(\lambda_o z)}{dz^f} dz$$

$$\rho\_Z_{c\xi}^{ef} = \int_0^h \rho(z) \frac{d^e \cos(\lambda_l z)}{dz^e} \frac{d^f \xi_k(z)}{dz^f} dz \qquad \text{(B.83-84)}$$

$$\rho\_Z_{\xi\xi}^{ef} = \int_0^h \rho(z) \frac{d^e \xi_t(z)}{dz^e} \frac{d^f \xi_k(z)}{dz^f} dz$$

$$T\_Z_{cc}^{ef} = \int_0^h -\frac{1}{2}(A+2B)\alpha(z,T) \frac{d^e \cos(\lambda_l z)}{dz^e} \frac{d^f \cos(\lambda_o z)}{dz^f} dz \qquad \text{(B.85)}$$

$$T\_Z_{c\xi}^{ef} = \int_0^h -\frac{1}{2}(A+2B)\alpha(z,T) \frac{d^e \cos(\lambda_l z)}{dz^e} \frac{d^f \xi_k(z)}{dz^f} dz \qquad \text{(B.86)}$$

$$T\_Z_{\xi c}^{ef} = \int_0^h -\frac{1}{2}(A+2B)\alpha(z,T) \frac{d^e \xi_t(z)}{dz^e} \frac{d^f \cos(\lambda_o z)}{dz^f} dz \qquad \text{(B.87)}$$

$$T\_Z_{\xi\xi}^{ef} = \int_0^h -\frac{1}{2}(A+2B)\alpha(z,T) \frac{d^e \xi_t(z)}{dz^e} \frac{d^f \xi_k(z)}{dz^f} dz \qquad \text{(B.88)}$$

where $e = 0,\ 1$ and $f = 0,\ 1$.

Acknowledgements

Conflict of Interest

The authors declare no conflict of interest.

Data Availability Statement

Research data are not shared.

Keywords

[1] M. Koizumi, *Composites Part. B* **1997**, *28*, 1.
[2] Y. Wang, W. Chen, X. Li, *Appl. Math. Mech.* **2015**, *36*, 581.
[3] B. Wu, M. Destrade, W. Chen, *Int. J. Mech. Sci.* **2020**, *187*, 106006.
[4] D. Liu, S. Kitipornchai, W. Chen, J. Yang, *Compos. Struct.* **2018**, *189*, 560.
[5] R. Moradi-Dastjerdi, K. Behdinan, *Appl. Math. Modell.* **2021**, *96*, 66.
[6] S. Chakraverty, K. K. Pradhan, *Aerosp. Sci. Technol.* **2014**, *36*, 132.
[7] S. H. Mirtalaie, *J. Dyn. Syst. Meas. Control Trans. ASME* **2018**, *140*, 101006.
[8] R. Lal, R. Saini, *Appl. Acoust.* **2020**, *158*, 107027.
[9] P. Malekzadeh, A. Alibeygi Beni, *Compos. Struct.* **2010**, *92*, 2758.
[10] A. G. Shenas, P. Malekzadeh, *Thin-Walled Struct.* **2016**, *106*, 294.
[11] A. G. Shenas, P. Malekzadeh, *Mech. Adv. Mater. Struct.* **2017**, *24*, 885.
[12] A. Shahrjerdi, F. Mustapha, S. M. Sapuan, M. Bayat, D. L. A. Abdul Majid, R. Zahari, *Key Eng. Mater.* **2011**, *471–472*, 133.
[13] P. P. Minh, N. D. Duc, *Thin-Walled Struct.* **2021**, *159*, 107291.
[14] J. Yang, H. S. Shen, *J. Sound Vib.* **2002**, *255*, 579.
[15] Y. Zhu, P. Shi, Y. Kang, B. Cheng, *Thin-Walled Struct.* **2019**, *144*, 106234.
[16] T. M. Tu, T. H. Quoc, N. Van Long, *Aerosp. Sci. Technol.* **2019**, *84*, 698.
[17] Q. Li, V. P. Iu, K. P. Kou, *J. Sound Vib.* **2009**, *324*, 733.
[18] P. Malekzadeh, S. A. Shahpari, H. R. Ziaee, *J. Sound Vib.* **2010**, *329*, 425.
[19] P. Shi, C. Y. Dong, *J. Sound Vib.* **2012**, *331*, 3649.
[20] T. E. Carmichael, *Q. J. Mech. Appl. Math.* **1959**, *12*, 29.
[21] P. A. A. Laura, R. Grossi, *J. Sound Vib.* **1978**, *59*, 355.
[22] P. A. A. Laura, R. O. Grossi, *J. Sound Vib.* **1979**, *64*, 257.
[23] P. A. A. Laura, R. O. Grossi, G. I. Carneiro, *J. Sound Vib.* **1979**, *63*, 499.
[24] D. J. Gorman, *J. Sound Vib.* **1990**, *139*, 325.
[25] P. A. A. Laura, R. H. Gutierrez, *J. Sound Vib.* **1994**, *173*, 702.
[26] W. L. Li, *J. Sound Vib.* **2004**, *273*, 619.
[27] J. Du, W. L. Li, G. Jin, T. Yang, Z. Liu, *J. Sound Vib.* **2007**, *306*, 908.
[28] G. Jin, Z. Su, S. Shi, T. Ye, S. Gao, *Compos. Struct.* **2014**, *108*, 565.
[29] K. Zhou, Z. Lin, X. Huang, H. Hua, *Appl. Acoust.* **2019**, *154*, 236.
[30] Z. Su, L. Wang, K. Sun, D. Wang, *Int. J. Mech. Sci.* **2019**, *157–158*, 872.
[31] Y. S. Touloukian, *Thermophysical Properties of High Temperature Solid Materials*, Macmillan, New York **1967**.
[32] J. N. Reddy, C. D. Chin, *J. Therm. Stresses* **1998**, *21*, 593.
[33] K. M. Liew, K. C. Hung, M. K. Lim, *Int. J. Solids Struct.* **1993**, *30*, 3357.
[34] K. M. Liew, K. C. Hung, M. K. Lim, *J. Appl. Mech. Trans. ASME* **1995**, *62*, 159.
[35] Y.-W. Kim, *J. Sound Vib.* **2005**, *284*, 531.
[36] Y. Chen, G. Jin, C. Zhang, T. Ye, Y. Xue, *Composites Part B* **2018**, *153*, 376.